Title
MANY-BODY EFFECTS IN X-RAY PHOTOEMISSION FROM MAGNESIUM

Authors
Ley, L.
McFeely, F.R.
Kowalczyk, S.P.
et al.

Publication Date
1974-05-01

Submitted to Physical Review B

LBL-2323
Preprint

MANY-BODY EFFECTS IN X-RAY PHOTOEMISSION FROM MAGNESIUM

L. Ley, F. R. McFeely,
S. P. Kowalczyk, J. G. Jenkin and D. A. Shirley

May 1974

Prepared for the U. S. Atomic Energy Commission
under Contract W-7405-ENG-48

DISCLAIMER

MANY-BODY EFFECTS IN X-RAY PHOTOEMISSION FROM MAGNESIUM*

L. Ley†, F. R. McFeely, S. P. Kowalczyk, J. G. Jenkin††, and D. A. Shirley

Department of Chemistry and
Lawrence Berkeley Laboratory
University of California
Berkeley, California 94720

May 1974

ABSTRACT

X-ray photoemission experiments were performed on samples of magnesium and aluminum prepared with atomically clean surfaces in ultrahigh vacuum. Core-level binding energies were in excellent agreement with x-ray emission data. Asymmetries in core-level peaks were observed and are compared with theory. The Mg KLL Auger spectrum showed kinetic energies higher than the literature values. Many-body effects, in the form of extra-atomic relaxation, were present in core levels and Auger lines. Both KL_1V and $KL_{23}V$ Auger peaks of Mg were observed. Many-body effects were also manifest as rich plasmon satellite structure accompanying every primary peak. The valence-band spectrum was compared with x-ray emission data and with the $KL_{23}V$ peak. The spectra were interpreted in terms of energy-level diagrams rather than one-electron "levels". It is argued that valence-band spectra obtained by different methods can be compared most directly among states with the same number of core holes. A hierarchical classification of hole states is suggested. The effect of the degree of localization of the hole-state on the relaxation energies in metals is discussed and shown to be small. Finally it was observed that in several light metals the energies required to remove a valence-band electron or a unipositive ion core are about equal.

I. INTRODUCTION

Photoemission from a metal is manifestly a many-body process, but the observed spectral features are usually labeled in terms of one-electron quantum numbers. When interpreting photoemission spectra it is important not to take the one-electron labels so literally as to neglect the omnipresent many-electron effects. Accordingly this paper, which reports a high-resolution x-ray photoemission study of magnesium (and a partial study of aluminum) under ultra-high vacuum conditions, is cast in a format that emphasizes the interplay between one-electron and many-electron aspects of each spectral feature. The advantage of this complementary point of view is underscored in most instances by superior agreement between theory and experiment when both aspects are considered.

Experimental procedures and results are given in Sec. II. "One electron" binding energies of core levels are discussed in Sec. III, with emphasis on many-electron relaxation effects. Asymmetries of these peaks are discussed and compared with theory. Auger peaks, which involve two-hole states, are discussed in Sec. IV, with relaxation effects again stressed. In Sec. V the valence band densities of states from photoemission, x-ray emission, and KLV spectra are compared. Hole-state localization is treated in Sec. VI. Finally, energy losses by unbound electrons through the creation of plasmons are reported in Sec. VII.

II. EXPERIMENTAL PROCEDURES AND RESULTS

These x-ray photoemission experiments were carried out in a Hewlett-Packard 5950A ESCA Spectrometer that had been modified for ultra-high-vacuum operation. Samples with atomically clean surfaces were prepared by vacuum evaporation of 99.95% pure magnesium or 99.999% pure aluminum in a sample preparation chamber having a base pressure of 3×10^{-9} Torr, followed by rapid transfer *in vacuo* to the analyzer chamber, which was maintained at 6×10^{-11} Torr, as measured on a nude Bayard-Alpert ion gauge. Photoemission was achieved by irradiating the sample with monochromatized $AlK\alpha_{1,2}$ x-rays (1486.6 eV).

Spectra covering the electron kinetic-energy range 200-1500 eV were taken first to insure sample purity. In addition to photoelectron lines expected from the atomic levels of Mg, there were KLL and KLV Auger lines in the 1050-1250 eV region. Also present were characteristic energy loss (plasmon) satellites associated with every line. The full-energy spectrum provided an effective *in-situ* chemical analysis of the first few atomic layers of the sample: i.e., those from which the electrons that appear in the full-energy lines are ejected. The absence of any lines that could not be attributed to Mg indicated the absence of any impurities in high concentrations. A careful study of the kinetic energy regions where the C(1s) and O(1s) peaks would be expected allowed us to set upper limits of 0.3 monolayers on the amount of each of these two elements present. Additional evidence for the surface cleanliness of the sample comes from two sources: the observation of a well-formed surface plasmon peak and the absence of oxide satellites on core-level peaks. Similar comments apply to the Al sample. Only the positions and shapes of the Al 2s and 2p core levels will be discussed in this paper,

for comparison with the Mg results. Characteristic binding energies or kinetic energies are given and discussed separately in the appropriate sections below.

III. CORE-LEVEL SPECTRA

A. One-Electron Core-Level Binding Energies

The 1s, 2s, and 2p spectra of Mg are shown in Fig. 1. Each core-level peak is accompanied by several plasmon loss peaks, which are discussed in Sec. VII. The core-level binding energies relative to the Fermi energy are denoted E_B^F. They are set out in Table I. Also given are values from an atomic energy level compilation by Bearden and Burr[1] and the $E_B^F(2p)$ value of 49.5 ± 0.1 eV which we have read from the x-ray spectrum published by Neddermeyer[2] (the ±0.1 eV error was assigned by us: it is our estimate of the uncertainty entailed in defining the Fermi energy E_F). The values of E_B^F from Ref. 1 are less accurate than ours, but more importantly they are higher by from 0.85 to 2.4 eV for the 1s, 2s, and 2p levels, while Neddermeyer's value for $E_B^F(2p)$ agrees within the 0.1 eV errors. We believe that this difference can be attributed to oxidation of the surface of the magnesium samples used in the earlier photoemission experiments from which Bearden and Burr's values were derived. Siegbahn, et al.,[3] emphasized the importance of this problem for active metals, and indicated that shifts of ∿ 2 eV in binding energy may be observed on oxidation. The recent photoemission results of Tejeda et al.[4] on clean surfaces agree with ours.

A good test of the accuracy of the photoemission binding energies is given by comparing them with x-ray energies in magnesium. X-ray energies are measured on bulk material and are therefore not sensitive to surface oxidation. An energy-level diagram that illustrates the connection between x-ray emission and x-ray photoemission energies is shown in Fig. 2. This diagram depicts the hole-state energy-level spectrum that is generated by ejecting an electron from a 1s, 2s, 2p, or valence-band orbital in magnesium.

The levels are the true many-particle energy levels of the system, with many-body relaxation energies, etc., included. The energies of these levels above the ground state are equal to the one-electron binding energies relative to the "vacuum level", E_B^V. Since the binding energy of an electron at the Fermi energy E_F is just the work function, ϕ, it follows that the binding energy of a core level i relative to E_F is given by

$$E_B^F(i) = E_B^V(i) - \phi \quad . \tag{1}$$

In our experiments the Fermi edge was clearly evident in the valence-band spectrum, so $E_B^F(i)$ was measured directly.

The energies of characteristic x-rays are given by the differences between pairs of binding energies. Thus, for example,

$$\begin{aligned} \Delta E(K\alpha_{12}) &= E_B^V(1s) - E_B^V(2p) \\ &= E_B^F(1s) - E_B^F(2p) \quad . \end{aligned} \tag{2}$$

Thus x-ray photoemission energies can be compared directly with x-ray emission energies. The values of E_B^F obtained in this work show excellent agreement with x-ray values, as indicated by columns 6 and 7 of Table I. Thus all three of our core-level energies for Mg--1s, 2s, and 2p--are in complete agreement with x-ray values.

The Al 2s and 2p binding energies agree only fairly well with x-ray values. This is attributable in part to the difficulty of assigning a consistent Fermi energy, and probably in part to an erroneous x-ray value for the 2s-2p transition.

The effect of surface oxidation on apparent core-level energies is illustrated in the right side of Fig. 2. The more positive environment of core-hole states in oxidized magnesium atoms increases the binding energies of these states relative to the reference energy E_F. The latter is unshifted in the surface-oxidized sample if no charge buildup occurs. Thus the apparent binding energies will be too large, as observed in the earlier Mg work (Table I, column 3).

Figure 3 shows the conventional ground-state one-electron "energy-level" diagram that has been used traditionally in discussing both x-ray emission and photoemission data.[5a,b] Since these one-electron "levels" do not really exist, this type of diagram is of course only an approximation to reality. As such, it can be very useful in discussing gross structure, such as the identities of transitions. In explaining subtle effects such as chemical shifts or many-body relaxation energies, however, in both of which the final state plays a large role, diagrams such as Fig. 3 are inadequate or even misleading. The reader can easily verify this statement by attempting to interpret the results reported in this paper using Fig. 3. We therefore advocate using diagrams like Fig. 2, which depict the true energy levels of the system. Parratt[5c] has discussed this point in more detail.

The measured core-level binding energies are in good agreement with theory. To make the comparison we must first add to $E_B^F(i)$ the measured work functions ϕ = 3.7 eV for Mg and 4.2 eV for Al[6] to obtain the "vacuum" binding energy $E_B^V(i)$, according to Eq. (1). The values of $E_B^V(i)$ so obtained are listed in Table II. Theoretical core-level binding energies for free atoms, $E_B^A(i)$, are also listed. These values were calculated by Siegbahn, et al.[7]

using an optimized Hartree-Fock-Slater approach devised by Rosén and Lindgren.[8] As relativistic hole-state calculations, these $E_B^A(i)$ values contain every sizable effect except electron correlation. A fairly accurate estimate of correlation effects on the 1s and 2s binding energies can be obtained by simply using results of Verhaegen, et al.[9] and of Moser, et al.,[10] for neon binding energies. Atomic binding energies of Mg and Al corrected in this way for correlation in the 1s and 2s cases, are listed as $E_B^A(i,corr)$ in Table II. These estimates of the atomic binding energies are believed to be accurate to 1.0 eV or better.

Comparison of the best estimates of the core-level binding energies in free atoms, $E_B^A(i,corr)$ (Table II, Col. 3) with the experimental values $E_B^V(i)$ for metallic Mg and Al (Table II, Col. 6) shows the latter to be lower by 4-8 eV. This is attributable to a many-body effect: the extra-atomic relaxation of conduction-band states toward the core-hole state during photoemission to form a semi-localized exciton state in which the positive charge of the hole is shielded.[11] A theoretical model that estimates the core-level binding-energy shift due to extra-atomic relaxation in terms of atomic two-electron integrals was described earlier.[12] Application of this model to Mg, for example, gives the estimates of extra-atomic relaxation energies due to the hole-state polarization potential

$$\langle 1s|V_p^{ea}|1s\rangle_{Mg} \cong [F^0(1s,3p) - \tfrac{1}{6}G^1(1s,3p)]_{Al}$$

$$\langle 2s|V_p^{ea}|2s\rangle_{Mg} \cong [F^0(2s,3p) - \tfrac{1}{6}G^1(2s,3p)]_{Al}$$

$$\langle 2p|V_p^{ea}|2p\rangle_{Mg} \cong [F^0(2p,3p) - \tfrac{1}{6}G^0(2p,3p) - \tfrac{1}{15}G^2(2p,3p)]_{Al} \quad .$$

Similar expressions apply to Al. The binding-energy shifts are then given by

$$E_B^V(\text{theo}) \cong E_B^A - \frac{1}{2}\langle V_p \rangle \quad . \tag{3}$$

Relaxation-energy shifts, estimated using this model and Mann's integrals,[13] are given in Table II, column 4. Column 5 lists theoretical estimates of E_B^V in Mg metal, after correction for this many-body screening effect. These values are to be compared to the experimental results in column 6. Considering the estimated accuracy of ±1.0 eV in $E_B^A(\text{corr})$ and the approximate nature of our relaxation model, the agreement is gratifying. Comparison of columns 3, 5, and 6 in Table II underlines the importance of extra-atomic relaxation and supports the above model as a reasonably accurate method for estimating the size of this effect.

B. Line Asymmetry

Another manifestation of many-body relaxation effects in the core-level photoemission is the asymmetry of the full-energy peaks. Following the earlier work of Mahan,[14] Anderson,[15] and others, which suggested that the coupling of the final-state hole to the conduction electrons could be an important effect in spectra involving electronic transitions in simple free-electron metals, there has been considerable discussion of this model,[16] particularly in reference to the theoretical understanding of experimental x-ray absorption and emission edges in Li, Na, Mg, and Al. Several alternative explanations have also been offered, principally by Dow and co-workers,[17] involving Auger and phonon broadening processes. Experimental data relevant to these questions have not kept pace with the theoretical developments.

Photoelectron spectra of core electron lines in metals offer the possibility for sensitive tests of the various theoretical models; in particular

it is expected that such electron lines will exhibit an asymmetry, being broader on the high binding-energy side. Citrin[18] and Hüfner et al.[19] have recently reported x-ray photoelectron spectra which exhibit this asymmetry to varying degrees in sodium and in a number of 4d and 5d metals, respectively. In the Mahan model[14,16] the asymmetry is due to the creation of low-energy conduction electron-hole pairs by the coupling of the final-state hole to the conduction electrons. This interpretation has been vigorously disputed by Dow et al.[17,20]

There is clearly a need for quantitative measurements of the asymmetry in XPS core-level spectra. Doniach and Sunjić have suggested[21] one simple way in which this may be accomplished; namely, by measuring the peak asymmetry index, the ratio of the absolute value of the peak energy minus the half height energy on the high binding-energy side to that on the low binding-energy side of the line. These authors have also furnished a table of the asymmetry index versus the singularity index α, where

$$\alpha = \sum_{\ell=0}^{\infty} 2(2\ell + 1)\left(\frac{\delta_\ell}{\pi}\right)^2 \quad ,$$

δ_ℓ being the phase shift of the ℓ^{th} partial wave for scattering of conduction electrons from the hole potential, in the spirit of the Mahan model.

Several Mg 2s line spectra taken in the present work have excellent statistics and are therefore amenable to accurate analyses of this type. There are no complications due to spin-orbit effects if one chooses a core s-level, and spectra were chosen for analysis only if there was clear evidence that the sample was uncontaminated by surface impurities such as oxygen, carbon, or water vapor. Average values for several Mg 2s line spectra are reported in

Table III, the quoted uncertainties being derived from the deviations of individual results from the mean.

It has been suggested to us[20,22] that the variation in asymmetry index with valency among the simple metals may be of even greater theoretical interest than the absolute values of such asymmetries. We have therefore re-examined s-core-level XPS spectra from pure samples of Al[23] and Li[23] with the results shown in Table III. Dow and Sonntag[24] have suggested an empirical prescription ($\alpha_0 \simeq 0.068\ r_s$) for calculating the Mahan exponent α_0 in terms of the electron-gas radius parameter r_s.[25] This was done for Al, Mg, and Na by use of the expression for α_ℓ obtained by Nozières and de Dominicis,[16] namely

$$\alpha_\ell = \frac{2\delta_\ell}{\pi} - \sum 2(2\ell + 1)\left(\frac{\delta_\ell}{\pi}\right)^2 = \frac{2\delta_\ell}{\pi} - \alpha$$

where $\ell = 0$ primarily; although the Li soft-x-ray absorption edge did not appear to follow this rule precisely.

The present results may be expressed in terms of the measured singularity indices α of Table III and α_0, calculated via r_s[25] and the rule $\alpha_0 \simeq 0.068\ r_s$,[24] see Table III. These results may then be compared with the form of the α versus α_0 curve as calculated from the phase shifts δ_ℓ.[20] Such a comparison is shown in Fig. 4. No simple relationship is apparent. A quantitative measure of the asymmetry in sodium would be of assistance in seeking to clarify this situation.

Recently Doniach[22] has pointed out to us that α may be explained in terms of the change in atomic potentials on core-level ionization. Using this concept, he has made the rough estimate $\alpha \sim 1/6$ for these simple metals, in fairly good agreement with the present experimental results.

IV. AUGER SPECTRA

A. The KLL Auger Spectrum

Figure 5 shows the rich KLL Auger spectrum of Mg, observed in the 1050-1250 eV kinetic energy range. This spectrum is superficially very different from the KLL Auger spectrum of Mg reported by Siegbahn, et al.[26] The differences can easily be understood, however, as arising from a rich plasmon spectrum present in Fig. 5 but absent in the earlier work, plus a shift of +5 eV in kinetic energy in our spectrum. This result is expected because the earlier work did not employ ultra high vacuum; thus the Mg surface must have been oxidized. This would account for both the absence of plasmons and the lower kinetic energies in the earlier work.

Using the relative kinetic energies reported for the various Auger peaks by Siegbahn, et al.,[26] together with the known plasmon energies and relative intensities (see Sec. VII), it is possible to locate all five Auger peaks corresponding to those reported by Siegbahn, et al. The KL_2L_3 (^1D), KL_1L_2 (^1P) and KL_2L_2 (^1S) assignments are obvious, while the KL_1L_1 (^1S) and KL_1L_3 (^3P) assignments follow from the anomalous intensities of the plasmon peaks with which they coincide. Derived energies are given in Table IV. Also given are the earlier values of Siegbahn, et al.[26] and a set of theoretical values that they calculated for free atomic Mg.

In comparing Auger energies in a metal with free-atom values, the relation

$$E^F(KLL) = E^A(KLL) + \phi + R_e(TA) \quad , \tag{4}$$

is expected to hold for each Auger component.[27] Here

$$E^A(KLL) = E^A(K) - E^A(LL) \quad ,$$

is the energy difference between the initial K-hole state and the final LL-hole state in the free atom, $E^F(KLL)$ is the Auger kinetic energy relative to E_F, and $R_e(TA)$ is the total Auger extra-atomic relaxation energy that results from differences in the screening-energy shifts of the two-hole and one-hole states that arise in the metal, as indicated in Fig. 6. Rearranging Eq. (4) we have

$$\begin{aligned} R_e(TA) &= E^F(KLL) - \phi - E^A(KLL) \\ &= E^V(KLL) - E^A(KLL) \quad , \end{aligned} \tag{5}$$

where $E^V(KLL)$ represents the Auger energy relative to the vacuum level. Values of $R_e(TA)$ derived from this relation are listed in Table IV.

To estimate theoretical values of $R_e(TA)$ we can use the model described by Kowalczyk, et al.,[27] in which the screening energy was approximated by atomic two-electron integrals. Applying that model to magnesium, we estimate $R_e(TA)$ as

$$R_e(TA)_{Mg} \cong 2\,\mathcal{F}(2p\ 3p)_{Si} - \tfrac{1}{2}\,\mathcal{F}(1s\ 3s)_{Al} \quad . \tag{6}$$

Here the equivalent-cores approximation has been used to estimate the two-electron integrals in the presence of core-level holes. This equation applies specifically to KLL' lines in which both the L and L' holes have 2p character. Other, similar, equations would describe $R_e(TA)$ for 2s-hole cases. In Eq. (6) the $\mathcal{F}$ terms describe two-electron multiplet interactions, as discussed in detail elsewhere. They have the form

$$\mathcal{F}(2p\ 3p) = F^0(2p\ 3p) - \frac{1}{6} G^0(2p\ 3p) - \frac{1}{15} G^2(2p\ 3p) \quad , \qquad (7)$$

etc. Mann's two-electron integrals were used for numerical estimates of $R_e(TA)$. Results are given in the last column of Table IV. These theoretical estimates are larger than the experimental values by factors of 1.3 to 1.8. This level of agreement is similar to that found earlier for other elements.[27] It indicates that the screening model is qualitatively correct, but that the screening valence electrons are, as expected, less localized in the metal than in the free atom.

B. KLV Auger Lines

Two additional low-intensity groups of peaks were observed slightly above the KLL group in kinetic energy (Fig. 5). We interpret these as arising from the KL_1V and $KL_{2,3}V$ Auger transitions plus their plasmon satellites. The mean $KL_{2,3}V$ transition energy is 1251.1 eV. Combining this with the one-electron K, L_{23}, and valence-band binding energies, we have[27]

$$E^F(KL_{2,3}V) = E_B^F(K) - E_B^F(L_{23}) - E_B^F(V) - \mathcal{F}(2p_c 3s_v) + R_e \quad . \qquad (8)$$

Here $\mathcal{F}(2p_c 3s_v)$ is the interaction energy between the 2p core hole and the 3s (valence-band) hole, and R_e is the extra-atomic relaxation energy arising from the interaction with the 3s hole of the screening charge attracted by the 2p hole, or vice versa. It is <u>not</u> the same as $R_e(TA)$, because part of $R_e(TA)$ is included in the empirical core-level binding energies. In fact $R_e \cong \frac{2}{3} R_e(TA)$.[27] Using $E^F(KL_{2,3}V)$ = 1251.1 eV, $E_B^F(K)$ = 1303.0 eV, $E_B^F(L_{23})$ = 49.4 eV, and $E_B^F(V)$ = 2.5 eV (an average value), we find

$$R_e - \mathcal{F}(2p_c 3s_v) = 0.0 \text{ eV} \quad .$$

This result states that interaction energy between a 2p and a 3s hole in the $KL_{23}V$ final state is equal to that between one of these holes and the screening charge. It is not clear a priori to what extents the 3s hole and the screening charge are localized, but this result shows that the two must be localized to a similar degree. If both were completely localized in 3s atomic orbitals, then $\mathcal{F}(2p_c 3s_v)$ would be given by

$$\mathcal{F}(2p_c 3s_v) \cong [F^0 - \frac{1}{6} G^1(2p\ 3s)]_{Al} = 12.5 \text{ eV} \quad ,$$

where Mann's integrals[13] were used for the numerical estimate. If the 3s hole and the screening charge were completely delocalized, R_e and $\mathcal{F}(2p_c 3s_v)$ would of course be much smaller.

There is independent evidence for the localized nature of the screening charge accompanying a 2p hole in Mg. In an earlier discussion[11] and (more accurately) from Table II, we found that the Mg(2p) binding energy was reduced by 3.2 eV in the metal relative to the free atom. This is interpreted as arising from dynamic extra-atomic relaxation due to screening. The corresponding static term would be twice as large, i.e., $R_e \cong 6.4$ eV. The large size of this term--about half the above atomic estimate--indicates that the screening charge associated with a 2p hole state in Mg is "semilocalized", in agreement with earlier conclusions.[11] Thus $\mathcal{F}(2p_c 3s_v) \cong 6.4$ eV in the $KL_{23}V$ final state, implying that the valence-band hole in this state is also partially localized on the Auger-active atom.

V. COMPARISON OF VALENCE-BAND SPECTRA

It is instructive to compare the shapes of the $KL_{23}V$ Auger peak with that of the valence-band peak in the x-ray photoemission spectrum and with the L_{23} x-ray emission profile, as all three peak shapes are determined by the valence-band density of states. To facilitate this comparison we note that the local density of states "on" a magnesium atom will be different when there is a core hole present than in the unperturbed metal. The excited hole states of the system can therefore be classified naturally according to the number of core hole states and valence-shell hole states present. This is illustrated in Fig. 7, in which states are labeled according to the type of hole present (e.g., $\overline{1}s$) and the core- and valence-hole "quantum numbers" C and V. The valence-band (local) density-of-states profile will be different for the C = 1 states than for C = 0 states because the core hole attracts a screening charge. We shall denote the density of states in the C = 1 level as $\rho_1(E)$ and in the C = 0 levels as $\rho(E)$. In this notation the selection rules are $\Delta(C + V) = 0$ for x-ray transitions and $\Delta(C + V) = +1$ for photoemission and Auger emission, with the former going upward and the latter downward in energy. The transitions with which we are concerned in Mg are shown in Fig. 8.

Valence-band photoemission to the $\overline{3}s(01)$ state proceeds within the C = 0 manifold: therefore it can in principle measure $\rho(E)$, in the approximation that effects such as cross-section variation across the band and differential final-state relaxation may be ignored. By this argument the experimental spectrum of the Mg valence bands (Fig. 8 top panel) should give a good representation of $\rho(E)$. We shall defer a discussion of whether or not it does, pending the outcome of cross-section calculations currently underway. We note

that the experimental spectrum does not have the simple shape that would naively be expected on the free-electron model; viz, a monotonic increase of intensity with energy to E_F and a sharp drop at E_F.

The $L_{2,3}$ x-ray emission spectrum of Neddermeyer[2] is reproduced in Fig. 8 (middle panel). The sharp peak at E_F in this spectrum has been variously attributed to a many-body effect--the Mahan anomaly--or to (one-electron) band-structure effects. There is no evidence whatever for such a peak in the photo-emission spectrum (the 0.55 eV FWHM instrumental resolution of our spectrometer would broaden such a peak if it were present, but could not obscure it completely). This does not necessarily mean that the peak could not be a band-structure effect, because the "local density-of-states" profile studied in the XPS experiment is that of the C = 0 states, with no core hole present. If variations in relaxation energy and cross-section effects across the band can be ignored, XPS would therefore yield $\rho(E)$. Under similar assumptions XES would give $\rho_1(E)$, since C = 1 in the initial state (the 2p hole state) in this case.

A better comparison can be made between the L_{23} XES spectrum (Fig. 8, middle panel) and a $KL_{2,3}V$ Auger line (Fig. 8, lower panel). In the $KL_{23}V$ Auger transition, both initial and final states belong to the C = 1 manifold. Thus, again neglecting cross-section and relaxation variation across the band, this line should measure $\rho_1(E)$, as does the XES spectrum.

The $KL_{23}V$ peak has approximately the same width as the other valence-band peaks (6-7 eV). Like them, it is relatively steep on the high-kinetic-energy (Fermi edge) side. Its shape differs in detail from those of the XPS and XES peaks, however. It shows no strong evidence for a peak at the Fermi edge (a shoulder is present), thus suggesting that the XES peak is a collective

effect rather than a density-of-states effect. In addition, the $KL_{2,3}V$ Auger peak is more peaked about 2 eV below the Fermi edge than are the XPS or XES peaks. We interpret this as evidence that the 2p hole state tends to attract valence states and concentrate them on the host Mg atom, yielding a peak in the density of states. It would be premature to interpret the valence-band spectra in Fig. 8 further at this time. We can, however, conclude that the x-ray anomaly probably arises from causes other than the density of states, that $\rho_1(E)$ differs from $\rho(E)$, showing the effect of screening of the 2p hole on the valence band, and that cross-section variation is important.

VI. ON HOLE-STATE LOCALIZATION

It is instructive to compare the valence-electron binding energies in free atoms with those in the corresponding metals. We wish to focus particularly on the question of hole-state localization and extra-atomic relaxation energy effects in the metals. The energy-level diagram appropriate for this comparison is shown in Fig. 9, for the particular case of sodium, a simple monovalent itinerant-electron metal. Optical atomic data[28] have been combined with the cohesive energy,[29] the work function,[30] and the valence bandwidth in constructing this figure.

Let us consider two features of Fig. 9, both of which obtain for metals generally: (1) The average binding energy of the least-bound electron is substantially less in the metal than in the free atom; i.e., $\overline{E_B^V} < E_B^A$, and (2) It takes about as much energy to remove an electron from the metal as it does a unipositive ion core; i.e. $\overline{E_B^V} \cong \overline{E_B^V}(M^+)$. Before proceeding, let us define $\overline{E_B^V}$, the average valence-electron binding energy relative to the vacuum level.

For monovalent metals $\overline{E_B^V}$ presents no problem; it is simply the work function, ϕ, plus the additional energy that it takes to reach the average energy in the valence-band final-state peak. For a free-electron band this gives

$$\overline{E_B^V} = \phi + (2/5)\ (E_0 - E_F) \quad .$$

Here E_0 is the binding energy of the most tightly-bound valence electron state (analogous to the "bottom" of the band in a one-electron initial-state description), and $E_0 - E_F$ is the total spectral (i.e., final-state) band width.

For divalent or trivalent free-electron metals such as Mg or Al a fairly consistent definition of $\overline{E_B^V}$ could be obtained by integrating the final-state valence-band profile (density of states) from E_F up to the energy at which 1/4 or 1/6, respectively, of the density-of-states area is used up. This is a somewhat arbitrary procedure. Its approximate validity can be appreciated by considering a limiting case in which the individual valence bands were nonoverlapping. In that case the least-bound orbital in the free atom would correspond to the valence band nearest E_F. With this approach the coefficient of $E_0 - E_F$ in the above equation would become 0.17 for divalent and 0.11 for trivalent free-electron metals.

We can now quantitatively evaluate the first observation above--that $\overline{E_B^V} < E_B^A$ for valence electrons in several light metals. The results are displayed in Table V. The difference $E_B^A - \overline{E_B^V}$ is always positive and ranges from 2 to 6 eV. Wigner and Bardeen[31] explained the magnitude of the work function (and thus this difference) in 1935. Their arguments were based on free-electron description and the Wigner-Seitz sphere model, and they considered only alkalis, obtaining good agreement with experiment. An interesting discussion of this model has been given by Haug.[32] Recently Lang and Kohn[33] have presented a theory for the work function based on an inhomogeneous electron gas model with pseudopotential corrections, and with surface effects treated carefully. Their theory predicted work functions of simple metals well (to within 5-10%) and those of noble metals fairly well (within 15-30%). Thus the decrease in valence electron binding energy from atoms to metals, or alternatively the value of the work function, is adequately explained on a free-electron model.

The second observation above--that $\overline{E_B^V} \cong \overline{E_B^V}(M^+)$, is deduced by comparing empirical values of E_B^V and $E_c + E_B^A$. Since the latter sum is the energy

required to remove an ion core M^+ and a valence electron from the metal, it follows that $E_B(M^+) = E_C + E_B^A - \overline{E_B^V}$, at least for an infinite solid. That $E_B(M^+) \cong \frac{1}{2}(E_C + E_B^A)$ as shown in Table V is less expected. It is satisfying in a rather qualitative way, referring to a model of free-electron metals on the "jellium" level, that ion cores and valence electrons should have nearly equal binding energies, because a positive or a negative charge is being removed from the jellium in the two cases.

On reflection the reason for this binding-energy similarity is not so obvious. Valence-electron emission from a simple metal is usually understood as being accompanied by negligible relaxation energy among the remaining electrons, because the electron leaves a smeared-out free-electron Bloch state. By contrast the ion core is manifestly localized, and its departure must be accompanied by substantial rearrangement of the remaining electrons.

Direct comparisons can also be made of the differences between core-level electron binding energies in atoms and metals,

$$\Delta E_B(\text{core}) = E_B^A(\text{core}) - E_B^V(\text{core}) \quad ,$$

and the differences between valence-electron binding energies,

$$\Delta E_B(v) = E_B^A(v) - E_B^V(v) \quad .$$

Such comparisons show that the "solid-state shifts", ΔE_B, decrease in a gradual manner in going from core to valence orbitals. There is no abrupt change in ΔE_B, nor does it approach zero for valence electrons. Since the core-level shifts were attributed to relaxation of the valence-electron

gas to screen the localized final-state core hole, one might be tempted to infer (incorrectly) from the above variation of ΔE_B that valence band holes were also localized, whereas Wigner and Bardeen[31] obtained good values for the work function by assuming the opposite--that the valence-electron hole is completely delocalized.

Before explaining this apparent contradiction, let us make two general observations. First, the distinction between core electrons and (free) valence electrons is somewhat arbitrary. Some bands in most metals should show properties intermediate between the two extremes. Second, if similar values of $\Delta E_B(v)$ or ϕ can be estimated using either localized- or delocalized-hole-state models, then agreement of experiment with these estimates does not carry implications about the degree of localization of the hole state. Although the Wigner-Bardeen[31] model, based on a hole in a free electron gas, produced work functions in good agreement with experiment, this does not necessarily imply that the hole state is delocalized. Even if the hole state is delocalized the "solid-state shift" will be about the same as for a localized hole, as we shall show below.

Let us first compute the work functions for several simple metals on the assumption that the valence-shell hole states are completely localized on single atoms. Referring to the energy-level diagram in Fig. 9, the expression for ϕ in an alkali metal is

$$\phi = E_c + E_B^A(v) - E_R - (\overline{E_{VB}} - E_F) \quad . \tag{9}$$

Here the cohesive energy per atom appears because the removal of one valence electron from a monovalent metal effectively breaks one atom's bonds. The

$E_B^A(v)$ term, which can be obtained from optical data, gives the energy required to remove a valence electron from an atom considered alone. The extra-atomic relaxation energy, E_R, has been discussed earlier, particularly in connection with core hole states. These three terms taken together give the average energy of the valence bands or levels, $\bar{E}_{VB}$. Since the complete valence-electron photoemission spectrum is usually available, the difference $(\bar{E}_{VB} - E_F)$ can be obtained empirically and subtracted to obtain the work-function energy ϕ. Assuming the valence-band hole to reside on a single atom, we can estimate the extra-atomic relaxation energy from atomic integrals as

$$\bar{E}_R(\text{Na}) \cong \frac{1}{2} F^0(3s,3s) \quad ,$$

for sodium, for example. Here the valence-band hole is assumed to be shielded by s-band valence electrons. The factor of 1/2 arises because this is a dynamic relaxation process. Table VI gives work functions calculated on this model. The results for monovalent metals agree quite well with experiment. Also given in Table VI are values calculated by Lang and Kohn[33] on an itinerant electron model.

For polyvalent metals this simple model can give qualitatively reasonable results, but it is not clear what fraction of the cohesive energy should be included in the expression for ϕ. If all of E_c is included, the values of ϕ estimated for Mg and Al (Table VI) are about one eV too high. If only a fraction of E_c is included the agreement would be improved.

It is no accident that this model gives estimates of ϕ very similar to those obtained from the Wigner-Bardeen model. In fact the terms in the expressions for ϕ in the two models can be related term by term, and it is instructive to do so. Equation (9) of the Wigner-Bardeen paper is, in their original notation,

$$\phi = I + H - \frac{2}{3} F - 0.6\ e^2/r_s + 0.458\ e^2/3r_s - e^2 r_s f'(r_s) + eD \quad . \quad (10)$$

Here their I and H are identical to our $E_B^A(v)$ and E_c, respectively. F is the mean kinetic energy of an electron above the bottom of the band. Since the band width is $\frac{5}{3}$ F, the $\frac{2}{3}$ F term is just the energy difference between the mean energy and the Fermi energy. This is exactly equivalent to our $(\bar{E}_{VB} - E_F)$ term, which measures the difference between the mean binding energy and that of the least-bound electron. The $0.6\ e^2/r_s$ and $0.458\ e^2/3r_s$ terms are Coulomb and exchange energies, respectively. The correlation energy term, in $f'(r_s)$, is not included in our simple approach (it could be), but it is small. Estimates of $e^2 r_s f'(r_s)$ for Na based on the Wigner-Bardeen model and the Böhm-Pines model give 0.11 eV and 0.14 eV, respectively. Finally the surface term eD, although interesting, is also relatively small. It could be included in our simple model but we shall omit it for brevity. Wigner and Bardeen[31] set D = 0. Lang and Kohn[33] have discussed the eD term in detail.

With the last two terms in Eq. (10) neglected and the first three identified with three in Eq. (8) the agreement of these two expressions for ϕ rests on the similarity between the remaining term in each; i.e., between E_R and $0.447\ e^2/r_s$ $(= 0.6\ e^2/r_s - 0.458\ e^2/3r_s)$. Both of these terms are made up of Coulomb and exchange contributions. The first describes the dynamic relaxation energy associated with valence-band electrons relaxing to shield an electron hole localized on a single atom. By analogy one would expect the second to be the dynamic relaxation energy of the valence band electrons relaxing to shield an itinerant electron hole (a "Coulomb hole" for the Coulomb energy and a "Fermi hole" for the exchange energy). That this is a

valid interpretation can easily be shown by re-deriving the Wigner-Bardeen result using this picture. We shall do so for the Coulomb energy. First we note that E_R for the localized-hole model is readily obtained as a matrix element of the "polarization potential" $V_p = V^* - V$ of Hedin and Johansson,[34] where V^* is the Coulomb potential with the hole present and V is the potential with the state occupied. Specifically,

$$E_R = \frac{1}{2} \langle i | V_p | i \rangle \quad ,$$

where i denotes the eigenstate of the electron in question. Applying this approach to the free-electron model and using the expression $3e^2/r_s - e^2r^2/2r_s^3$ as the potential due to the s sphere, we find, on integrating over the s sphere, a Coulombic relaxation energy

$$\frac{1}{2}\left[\int_0^{r_2} 4\pi r^2 (3e^2/2r_s - e^2r^2/2r_s^3)\,dr\right]\left[4\pi r_s^3/3\right]^{-1} = 0.6\ e^2/r_s \quad .$$

This is of course the result given by Wigner and Bardeen, but derived from the point of view of relaxation of the valence-electron gas toward the itinerant hole state.

A numerical comparison of the relaxation energies calculated on the two models is very encouraging. For Na, the values are

Localized 3s hole state:

$$E_R = \frac{1}{2} F^0(3s,3s)_{\text{Atomic Na}} = 2.93 \text{ eV} \quad .$$

Delocalized hole state:

$$E_R = 0.6\ e^2/r_s - 0.458\ e^2/3r_s = 3.05 \text{ eV} \quad .$$

Similar agreement is obtained for other alkali metals (Table VII).

We may summarize this section by noting that the binding energy accompanying the removal of a charged particle from a metal contains a many body term--the relaxation energy arising from polarization of the electron gas toward (or away from) the resultant hole. This relaxation energy amounts to a few electron volts and is not strongly dependent on whether the particle is a (monovalent) ion core, a core electron, or a valence electron. From the similarity of the last two cases we can draw two imporant conclusions: (1) Differential relaxation across the valence band is likely to be small in metals. Therefore this effect should not cause large discrepancies between initial densities of states and photoemission spectra. (2) Relaxation energies are not strongly dependent on the degree of localization of the hole state, and therefore vary not only continuously, but little, from core- to valence-electron states. Explanation of the work function in terms of relaxation of the electron gas about a "Coulomb hole" closes a possible conceptual hiatus between core-electron binding energies, which are well-known to have a contribution from extra-atomic relaxation, and valence-electron binding energies, which are sometimes regarded as having no relaxation contribution because the valence electrons are delocalized in the initial state. We do not suggest that valence-electron holes in simple metals are in fact localized; the above discussion simply shows that the existence of a relaxation-energy term, and the value of the work function has little bearing on this question.

VII. PLASMON LOSS SPECTRA

Each distinct spectral feature arising from an electron being ejected from the Mg and Al samples showed characteristic satellite structure corresponding to energy losses by some electrons through the formation of plasmons of characteristic energies. Only the Mg plasmons will be discussed here, as the Al plasmons have been reported before.[23] Plasmon formation is a well-understood many-body effect.

Even the valence band peak in Mg had three identifiable plasmon satellites, as shown in Fig. 10. Also shown is the best-resolved plasmon structure that we were able to obtain in this work, on the 2p line of Mg. The asymmetric shape of the first bulk plasmon peak is evident. The surface plasmon peak is clearly resolved from the bulk plasmon peak, and a peak that we can assign to one bulk plus one surface plasmon ($P_1 + P_S$ in Fig. 10) is partially resolved. Since this work was carried out on a polycrystalline source with a wide acceptance angle, the energy resolution is not comparable to that available from electron energy-loss studies, but reliable plasmon energies can nevertheless be obtained. Derived plasmon energies are set out in Table IX. Our weighted average values of

$$\hbar\omega_p(\text{surface}) = 7.3(1)\ \text{eV}$$

$$\hbar\omega_p(\text{bulk}) = 10.7(1)\ \text{eV} \quad ,$$

are in excellent agreement with the values of 7.1 and 10.6 eV given by Powell and Swan.[35] Our ratio

$$\frac{\omega_p(\text{bulk})}{\omega_p(\text{surface})} = 1.47 \quad ,$$

is slightly smaller than theirs (1.49), but still well above the value $\sqrt{2}$ expected on the simplest theory.

ACKNOWLEDGMENTS

It is a pleasure to acknowledge helpful discussions and correspondence with Professors S. Doniach and J. D. Dow on the core-peak asymmetry problem. One of us (DAS) wishes to acknowledge an illuminating discussion with J. R. Schrieffer on the question of continuity in the relaxation energies between localized core holes and delocalized valence holes.

FOOTNOTES AND REFERENCES

*Work performed under the auspices of the U. S. Atomic Energy Commission.

†IBM Fellow.

††On leave from LaTrobe University, Australia.

1. J. A. Bearden and A. F. Burr, Rev. Mod. Phys. 39, 125 (1967); J. A. Bearden, Rev. Mod. Phys. 39, 78 (1967).

2. H. Neddermeyer, in "Electronic Density of States", NBS Special Publication 323 (1971), p. 313.

3. K. Siegbahn, C. Nordling, A. Fahlman, R. Nordberg, K. Hamrin, J. Hedman, G. Johansson, T. Bergmark, S.-E. Karlsson, I. Lindgren, and B. J. Lindberg, ESCA - Atomic, Molecular and Solid State Structure by Means of Electron Spectroscopy, Nova Acta Regiae Soc. Sci. Upsaliensis Ser. IV, Vol. 20 (1967), Appendix 1.

4. J. Tejeda, M. Cardona, N. J. Shevchik, D. W. Langer, and E. Schönherr, Phys. Stat. Sol. (b) 58, 189 (1973).

5. (a) D. H. Tomboulian, in Handbuch der Physik, ed. by S. Flügge (Springer-Verlag, Berlin, 1957), Vol. XXX, p. 258. (b) Reference 3, p. 36. (c) L. G. Parratt, Rev. Mod. Phys. 31, 616 (1959).

6. American Institute of Physics Handbook, Third Edition (McGraw-Hill, 1972), pp. 9, (172-180).

7. Reference 3, Appendix 2.

8. A. Rosén and I. Lindgren, Phys. Rev. 176, 114 (1968).

9. G. Verhaegen, J. J. Berger, J. P. Desclaux, and C. M. Moser, Chem. Phys. Letters 9, 479 (1971).

10. C. M. Moser, R. K. Nesbet, and G. Verhaegen, Chem. Phys. Letters 12, 230 (1971).

11. L. Ley, S. P. Kowalczyk, F. R. McFeely, R. A. Pollak, and D. A. Shirley, Phys. Rev. B 8, 2392 (1973).

12. Reference 11, Sec. IV, especially Eq. (14) and (15).

13. J. B. Mann, "Atomic Structure Calculations. I. Hartree-Fock Energy Results for the Elements Hydrogen to Lawrencium", Los Alamos Scientific Laboratory Report LASL-3690 (1967).

14. G. D. Mahan, Phys. Rev. 153, 882 (1967), and Phys. Rev. 163, 612 (1967).

15. P. W. Anderson, Phys. Rev. Letters 18, 1049 (1967).

16. See for example, P. Nozières and C. T. de Dominicis, Phys. Rev. 178, 1097 (1969); G. A. Ausman and A. J. Glick, Phys. Rev. 183, 687 (1969); G. D. Mahan, Solid State Phys. 29 (in press); and S. Doniach, P. M. Platzman, and J. T. Yue, Phys. Rev. B4, 3345 (1971).

17. See for example, J. D. Dow, J. E. Robinson, and T. R. Carver, Phys. Rev. Letters 31, 759 (1973); J. D. Dow and B. F. Sonntag, Phys. Rev. Letters 31, 1461 (1973); D. L. Smith and J. D. Dow, Phys. Rev. B9 (in press); and J. D. Dow et al. (several papers to be published).

18. P. H. Citrin, Phys. Rev. B 8, 5545 (1973).

19. S. Hüfner, G. K. Wertheim, D. N. E. Buchanan, and K. W. West, Phys. Letters 46A, 420 (1974).

20. J. D. Dow and D. R. Franceschetti, private communications.

21. S. Doniach and M. Sunjić, J. Phys. C: Solid State Phys. 3, 285 (1970).

22. S. Doniach, private communication.

23. R. A. Pollak, L. Ley, F. R. McFeely, S. P. Kowalczyk, and D. A. Shirley, J. Electr. Spectrosc. (in press).

24. J. D. Dow and B. F. Sonntag, Phys. Rev. Letters 31, 1461 (1973).

25. A table of r_s for various metals has been given by C. Kittel, Introduction to Solid State Physics (Wiley, New York, 1971), 4^{th} ed., p. 248.

26. Reference 3, p. 152.

27. S. P. Kowalczyk, L. Ley, F. R. McFeely, R. A. Pollak, and D. A. Shirley, Phys. Rev. B 9, 381 (1974).

28. C. E. Moore, "Atomic Energy Levels", NBS Circular 467, Volume I (U.S. Department of Commerce, 1949), p. 106.

29. L. Brewer, in High-Strength Materials, ed. by V. F. Zackay (John Wiley and Sons, Inc., New York, 1965), p. 12.

30. Reference 6, p. 280.

31. E. Wigner and J. Bardeen, Phys. Rev. 48, 84 (1935).

32. Albert Haug, Theoretical Solid State Physics (Pergamon Press, Oxford, 1972).

33. N. D. Lang and W. Kohn, Phys. Rev. B 3, 1215 (1971).

34. L. Hedin and G. Johansson, J. Phys. B 2, 1336 (1969).

35. C. J. Powell and J. B. Swan, Phys. Rev. 116, 81 (1959).

Table I. Magnesium and aluminum core-level binding energies and differences (in eV).

nℓ	E_B^F This work	Ref. 1	E_B^F Ref. 2	Ref. 4	$E_B(n\ell) - E_B(L_{2,3})$ This work	$E_B(n\ell) - E_B(L_{2,3})$ x-ray, Ref. 1	$E_B(n\ell) - E_B(L_{23})$ Ref. 3
Mg 1s	1303.0(1)	1305.4(4)	--	1303.0(2)	1253.6(1)	1253.60(2)	1256
Mg 2s	88.55(10)	89.4(4)	--	88.5(2)	39.15(10)	39.2(1)	38
Mg 2p	49.4(1)	51.4(5)	49.5(1)	49.6(2)	--	--	--
Al 2s	117.99(6)	117.7(4)	--	--	45.15(9)	42.80(15)	44.7
Al 2p	72.84(6)	73.1(5)	--	--	--	--	--

Table II. Comparison of core level binding energies in Mg and Al with theory.[a]

$n\ell$	$E_B^A(n\ell)$[b]	$E_B^A(n\ell,\text{corr})$[c]	$\frac{1}{2}\langle n\ell\|V_p\|n\ell\rangle$[d]	$E_B^V(n\ell,\text{theory})$	$E_B^V(n\ell,\text{expt})$
Mg 1s	1312	1312.6	5.1	1307.5	1306.7(1)
Mg 2s	97.7	96.6	4.9	91.7	92.25(10)
Mg 2p	56.3	--	4.9	51.4	53.1(1)
Al 1s	1569	1569.6	6.3	1563.3	1562.4(5)[e]
Al 2s	128	126.9	6.0	120.9	122.2(2)
Al 2p	80.6	--	6.0	74.6	77.0(2)

[a] All energies are given in eV.

[b] From Ref. 7.

[c] Using correlation corrections for neon from Refs. 9 and 10.

[d] See Ref. 12.

[e] From x-ray absorption data by K. Langer, Soft X-Ray Band Spectrum, ed. by D. J. Fabian (Academic Press, 1968), p. 62. Error estimate is ours.

Table III. Asymmetry of XPS core-level lines.

Line	Asymmetry index	α	r_s (Ref. 25)	α_0 (Ref. 24)
Mg 2s	1.27 ± 0.04	0.132 ± 0.012	2.65	0.180
Al 2s	1.35 ± 0.02	0.161 ± 0.008	2.07	0.141
Li 1s	1.42 ± 0.10	0.18 ± 0.03	3.25	0.221

Table IV. KLL Auger energies in magnesium (in eV).

Transition	E^F(KLL) Ref. 14	E^F(KLL) This work	E^V(KLL) This work	E^A(KLL) Ref. 26	R_e(TA)	R_e(TA) Theo.
KL_1L_1 (^1S)	1101	1106.0(3)	1102.3(3)	1088	14.3	18.9
KL_1L_2 ($^1P_1$)	1135	1139.8(2)	1136.1(2)	1123	13.1	18.9
KL_1L_3 ($^3P_{0,1,2}$)	1150	1154.3(6)	1150.6(6)	1137	13.6	18.9
KL_2L_2 (^1S)	1175	1179.8(2)	1176.1(2)	1165	11.1	18.9
KL_2L_3 (^1D)	1180	1185.3(2)	1181.6(2)	1171	10.6	18.9
KL_3L_3 ($^3P_{0,2}$)	not obs.	not obs.	--	1175	--	18.9

Table V. Valence-electron binding energies in atoms and solids (in eV).

Element, $n\ell$	$E_B^A(n\ell)$ [a]	E_c [b]	$e\phi$ [c]	$\overline{E_B^V}$ [d]	$\frac{1}{2}(E_B^A + E_c)$	$E_B(M^+)$	$\overline{E_B^V}(\text{corr})$ [e]	$E_R(\text{expt})$ [f]	$E_R(\text{theo})$ [g]
Li 2s	5.39	1.66	2.4	3.4	3.53	3.65	1.7	3.7	3.1
Na 3s	5.14	1.11	2.3	3.34	3.13	2.92	2.78	2.4	2.9
Mg 3s	7.64	1.52	3.7	4.86	4.58	4.30	4.09	3.5	2.9
Al 3p	5.98	3.35	4.2	4.9	4.67	4.43	3.8	2.2	3.5

[a] Reference 28.

[b] Obtained from ΔH_V (in Ref. 29) by $E_c = \Delta H_V - RT$.

[c] Reference 6.

[d] Derived from x-ray emission data (e.g. Ref. 5) and photoemission results as described in text.

[e] Corrected for (bond energy) ÷ (number of valence electrons).

[f] $E_B^A - \overline{E_B^V}(\text{corr})$.

[g] See text and Ref. 11.

Table VI. Calculated and experimental work functions (in eV) of Li, Na, Mg, and Al.

	φ_{loc} [a]	$\varphi_{non\text{-}local}$ [b]	φ_{expt} [c]
Li	2.95	3.37, 2.33	2.4
Na	2.31	2.83	2.3
Mg	5.10	4.05(0001 face)	3.7
Al	4.63	3.97	4.2

[a] From Eq. (9).

[b] From Ref. 33. An average of values for crystal faces is quoted here, except for Mg.

[c] From Ref. 6.

Table VII. Relaxation energies accompanying valence-electron ionization in alkali metals, based on localized and nonlocalized hole models. Energies are in eV.

Metal (ns)	$E_R(\text{loc}) \cong \frac{1}{2} F^0(\text{ns ns})$ [a]	$E_R(\text{itin}) = 0.447\ e^2/r_s$ [b]
Li(2s)	3.18	3.71
Na(3s)	2.93	3.05
K(4s)	2.34	2.45
Rb(5s)	2.18	2.32
Cs(6s)	1.95	2.16

[a] Using Mann's integrals (Ref. 13).

[b] Wigner-Bardeen model, with r_s values from Ref. 33.

Table VIII. Plasmon energies in magnesium (in eV).

Primary Peak	Kinetic Energy of Primary	P_S	P_1	P_2	P_3
2p	1437	7.3(1)	10.7(1)	21.5(2)	--
2s	1398	7.4(3)	10.7(1)	21.6(2)	--
1s	183	7.2(3)	10.9(4)	21.8(4)	32.0(5)
KLL (^1D)	1185	--	10.8(1)	21.3(2)	--
KLL (^1P)	1140	--	10.6(1)	21.9(5)	--
Valence band	1483	--	$\sim$ 10.8	$\sim$ 21.4	$\sim$ 32
Wgtd. Ave.		7.3(1)	10.7(1)	21.4(1)	

FIGURE CAPTIONS

Fig. 1. The 1s, 2s, and 2p x-ray photoemission spectra of atomically clean Mg metal, showing plasmon structure. Binding energies are given relative to E_F.

Fig. 2. The x-ray energy level diagram for magnesium metal and for surface-oxidized magnesium. Photoemission transitions are drawn on the left and x-ray emission lines are shown with arrows pointing down. Oxidation of the surface removes electrons from Mg atoms, creating a more positive environment for core-hole final states in photoemission and raising their energies as shown relative to E_F.

Fig. 3. The one-electron "energy-level" diagram that is conventionally used for discussing x-ray emission and photoemission.

Fig. 4. Values of the singularity index α as a function of the Mahan exponent α_0 from the present experimental results (·) and from the calculations of Dow and Franceschetti (Ref. 20), shown ——. See the text for details.

Fig. 5. The KLL and KLV Auger spectrum of atomically clean Mg metal. In the KLL spectrum only primary peak designations are given. In some cases these coincide or overlap with plasmon peaks.

Fig. 6. Effect of extra-atomic relaxation energies on one- and two-hole states in Mg KLL Auger transitions is depicted. The energy-level scale is only schematic, and shifts that cancel between the atom and metal are not shown. The extra-atomic screening energy of the two-hole state should be about four times that of the one-hole state.

Fig. 7. Schematic comparison of shapes of $KL_{23}V$ Auger peaks with XPS spectrum and L_{23} emission spectra. The various states involved are classified using C and V "quantum numbers" as explained in Sec. V of text.

Fig. 8. Upper panel: XPS valence band of Mg (this work).

Middle panel: L_{23} x-ray emission spectrum (from Ref. 2).

Lower panel: Mg $KL_{2,3}$ Auger spectrum (this work).

Fig. 9. Energy-level diagram relating the binding energy of a 3s electron in atomic Na to that of a 3s atom in the metal valence band.

Fig. 10. Plasmon structure on the valence-band peak (top) and the 2p peak (bottom). Note scale changes.

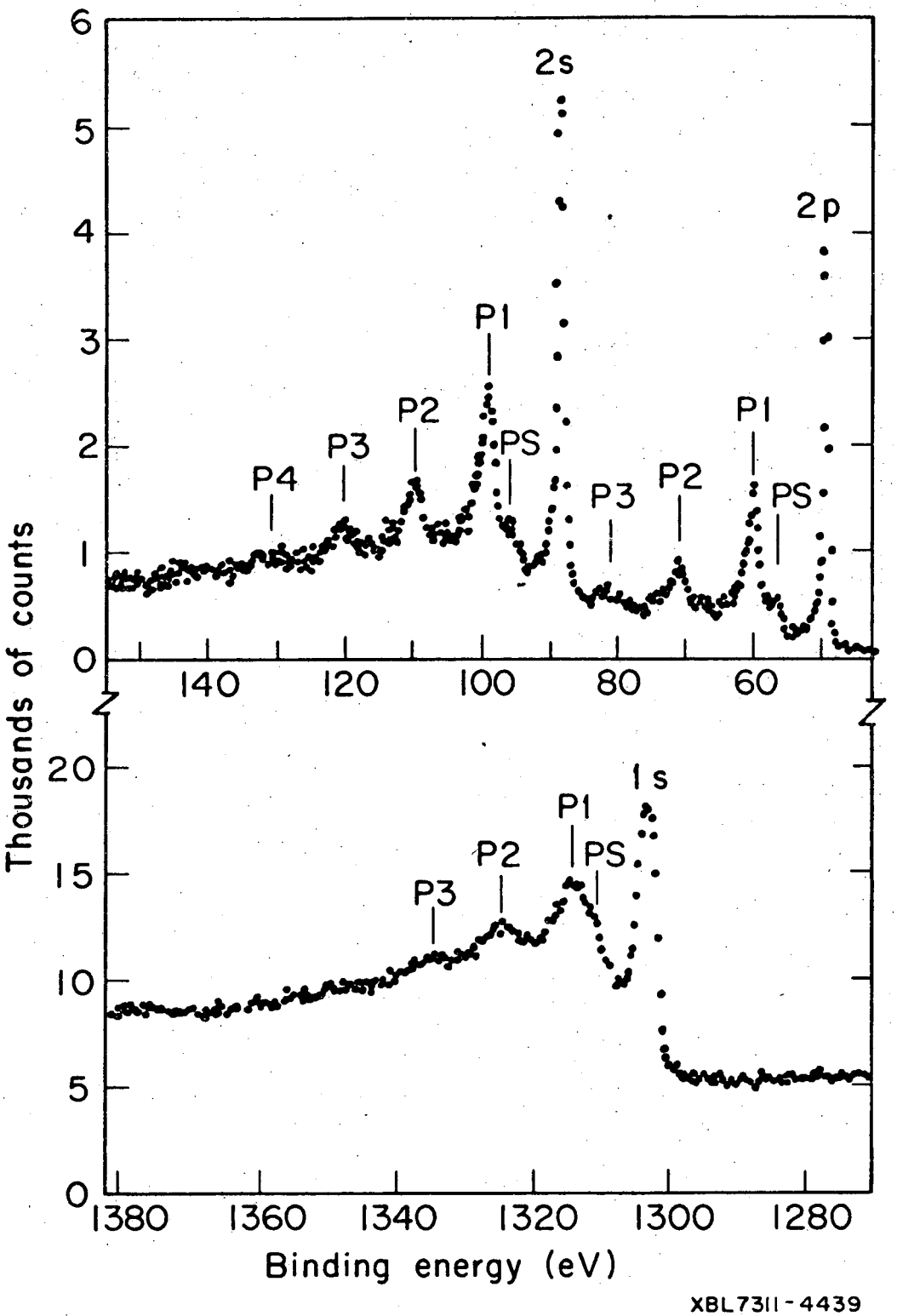
Thousands of counts
Binding energy (eV)
2s
2p
P1
P2
P3
P4
PS
1s
XBL7311-4439

Fig. 1

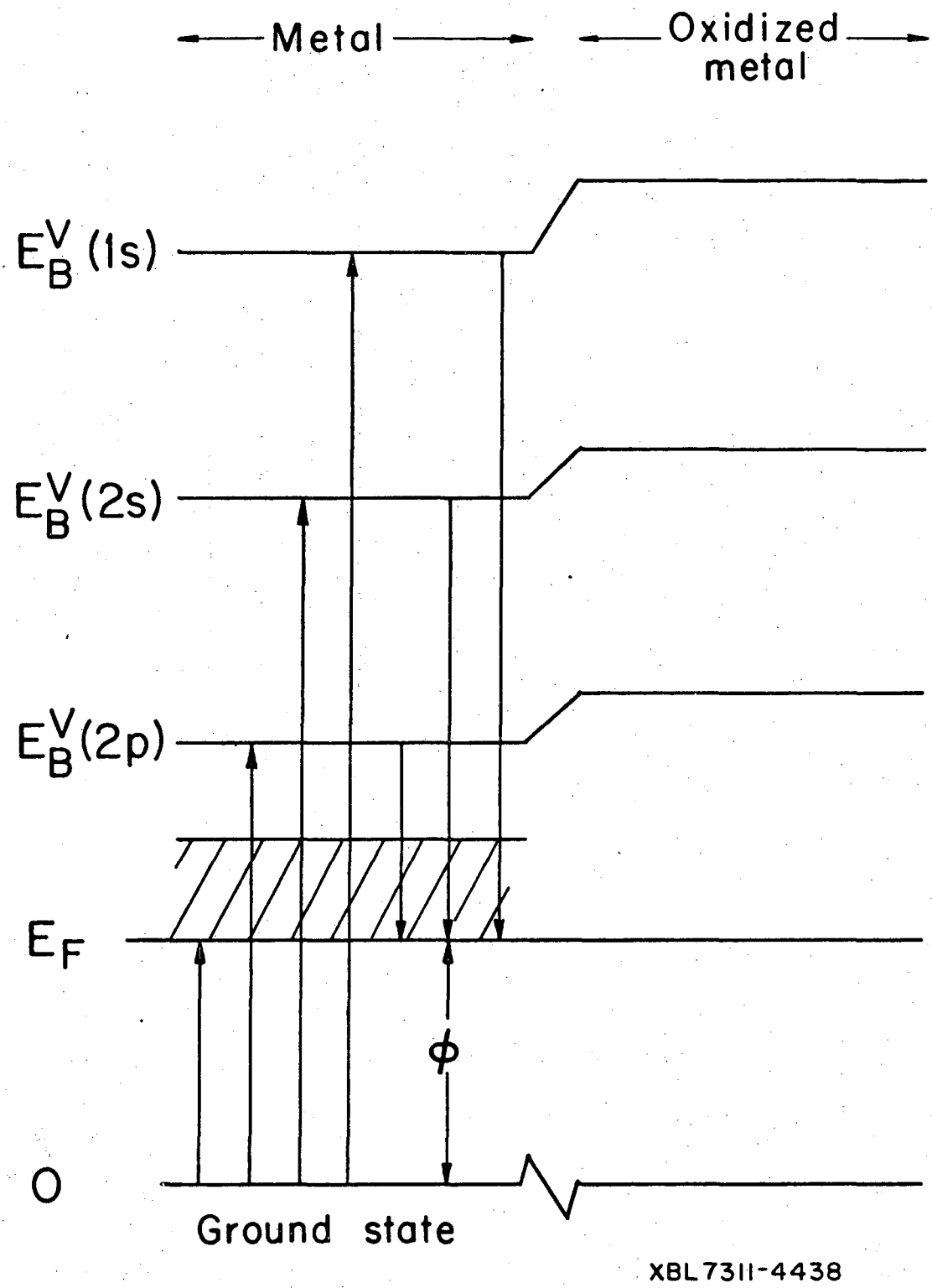
Metal
Oxidized metal
E_B^V (1s)
E_B^V (2s)
E_B^V (2p)
E_F
ϕ
0
Ground state
XBL7311-4438

Fig. 2

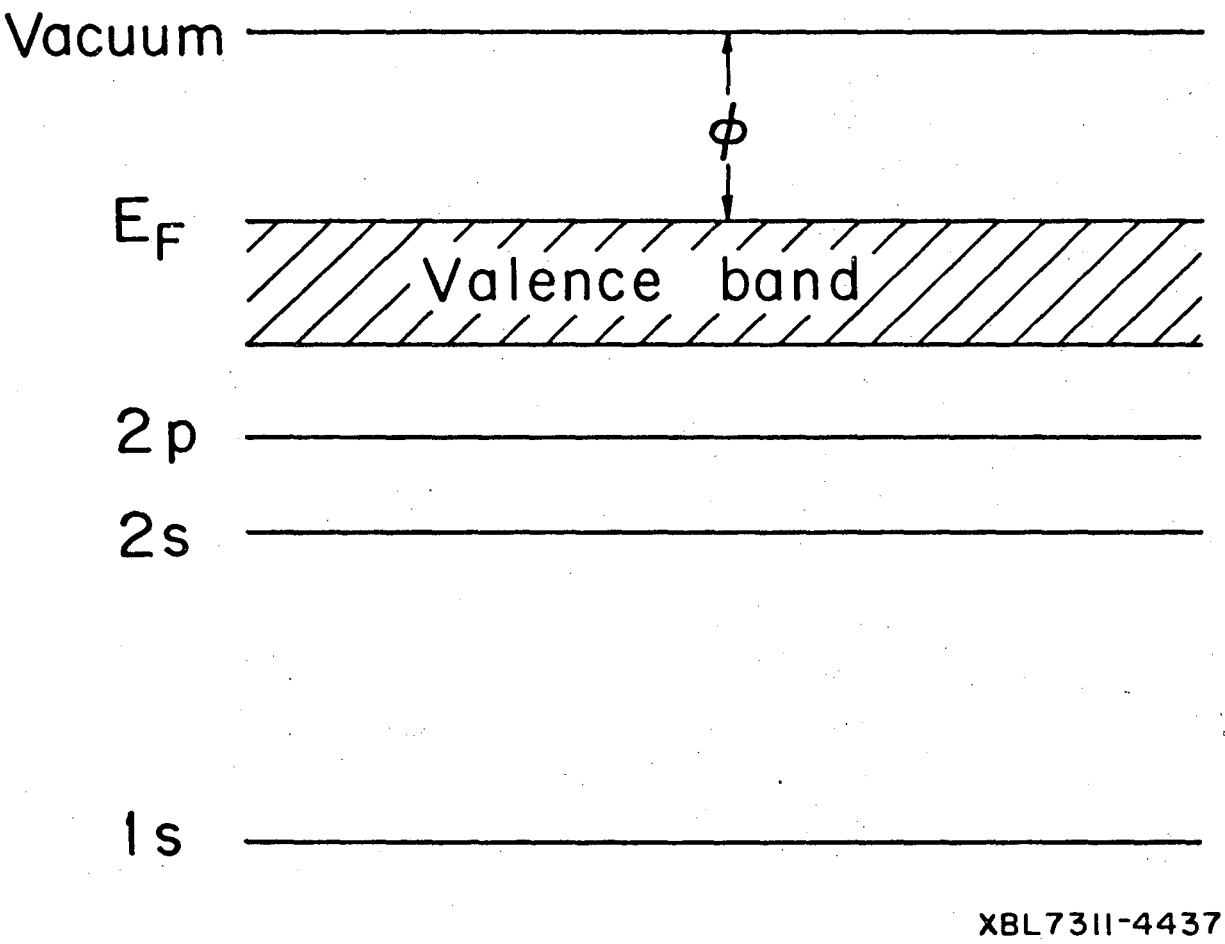

XBL7311-4437

Fig. 3

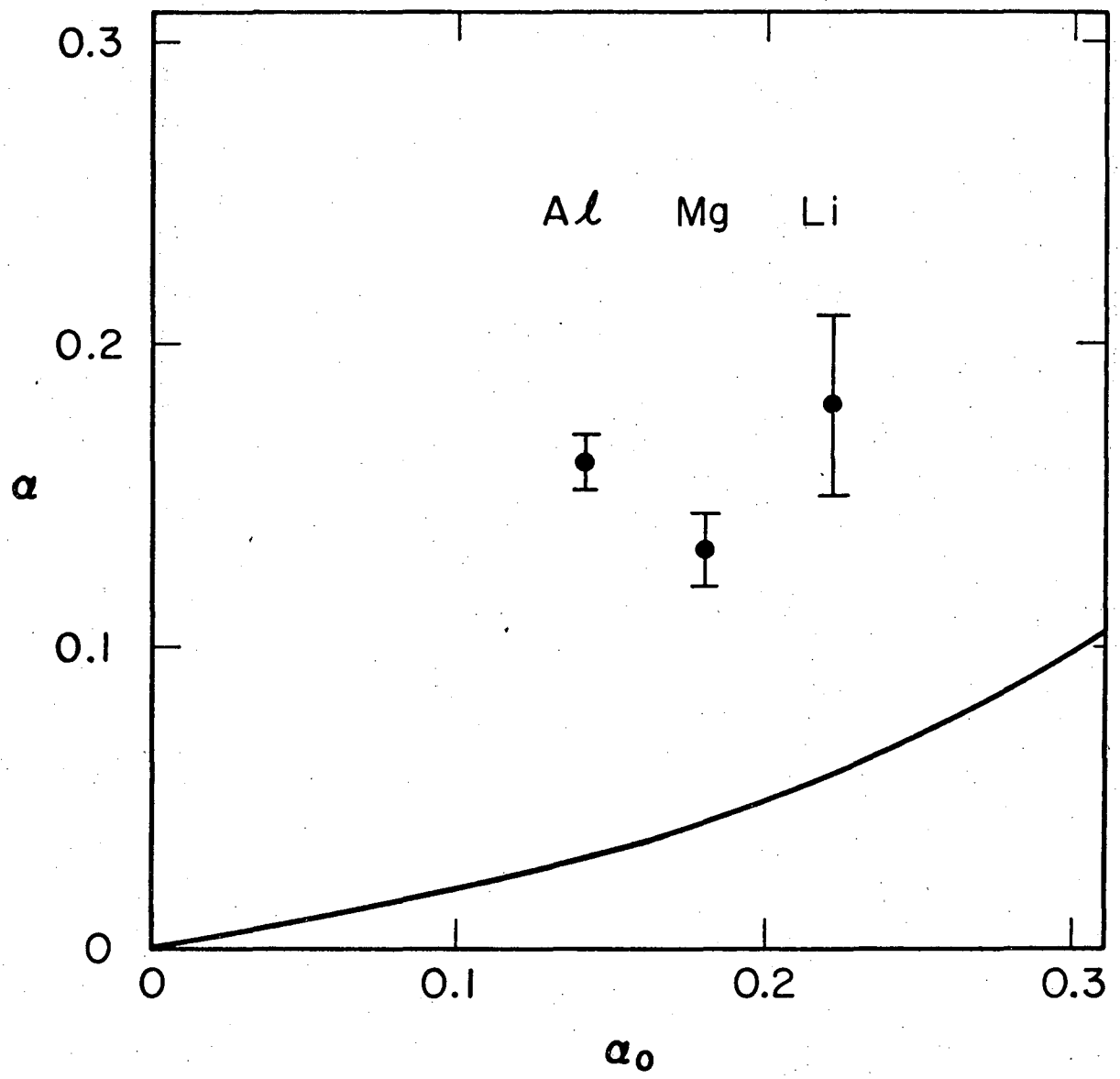

XBL 744-2889

Fig. 4

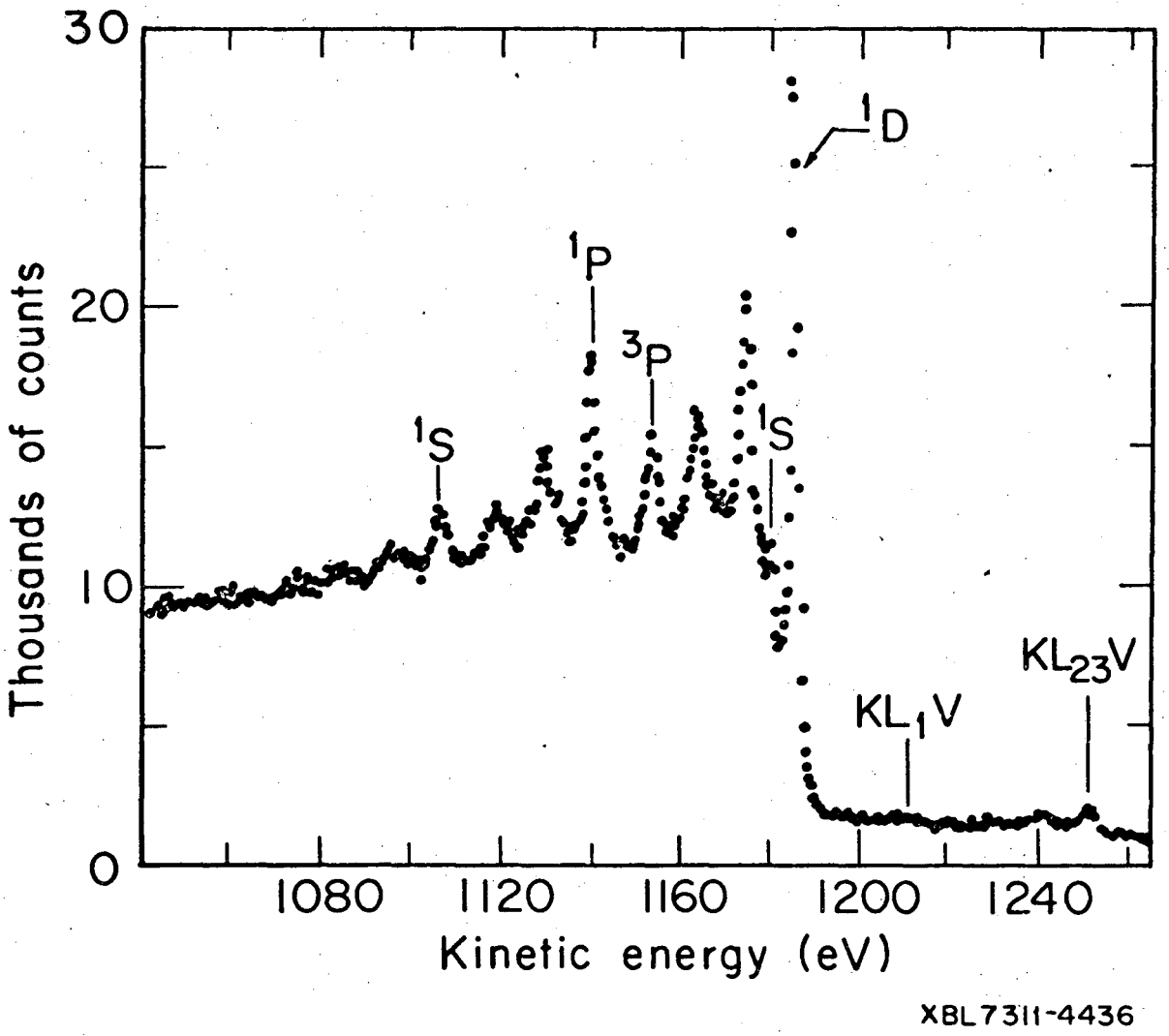
30
20
10
0
Thousands of counts
1D
1P
3P
1S
1S
KL1V
KL23V
1080
1120
1160
1200
1240
Kinetic energy (eV)
XBL7311-4436

Fig. 5

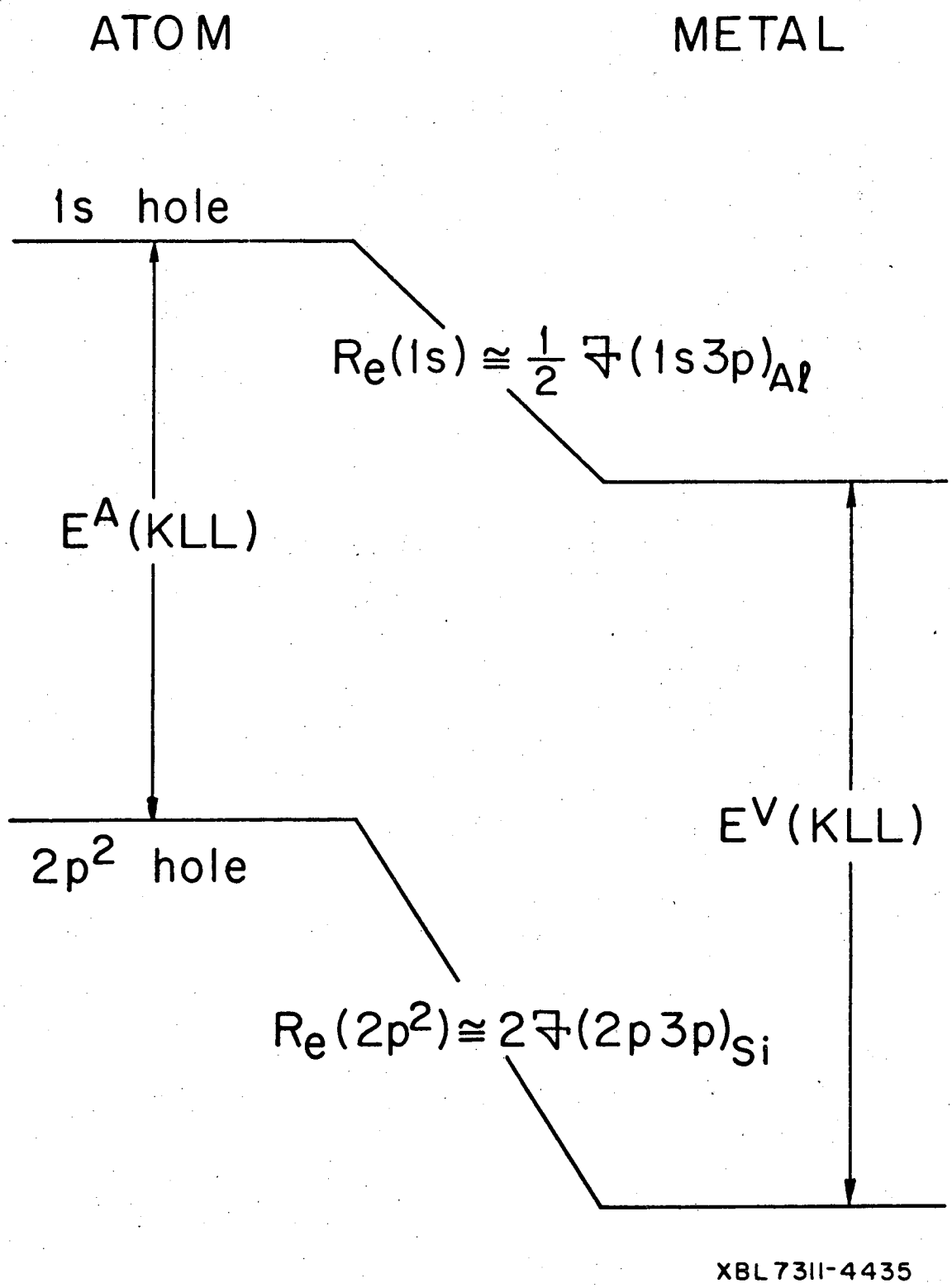
ATOM
METAL
1s hole
$R_e(1s) \cong \frac{1}{2} \mathcal{F}(1s3p)_{Al}$
$E^A(KLL)$
$E^V(KLL)$
$2p^2$ hole
$R_e(2p^2) \cong 2\mathcal{F}(2p3p)_{Si}$
XBL7311-4435

Fig. 6

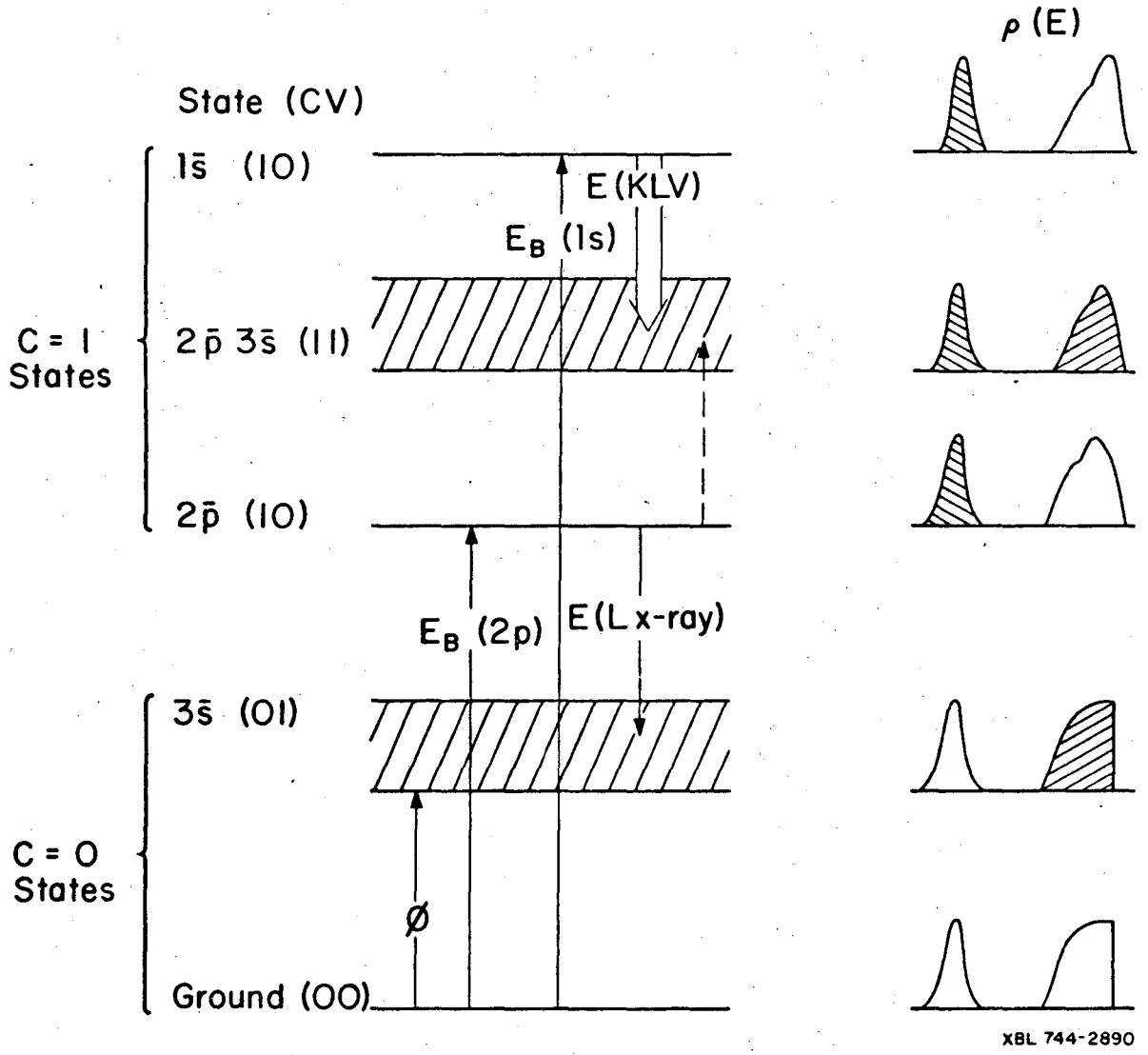
ρ (E)
State (CV)
1s̄ (10)
E(KLV)
E_B (1s)
C = 1
States
2p̄ 3s̄ (11)
2p̄ (10)
E_B (2p)
E(L x-ray)
3s̄ (01)
C = 0
States
Ø
Ground (00)
XBL 744-2890

Fig. 7

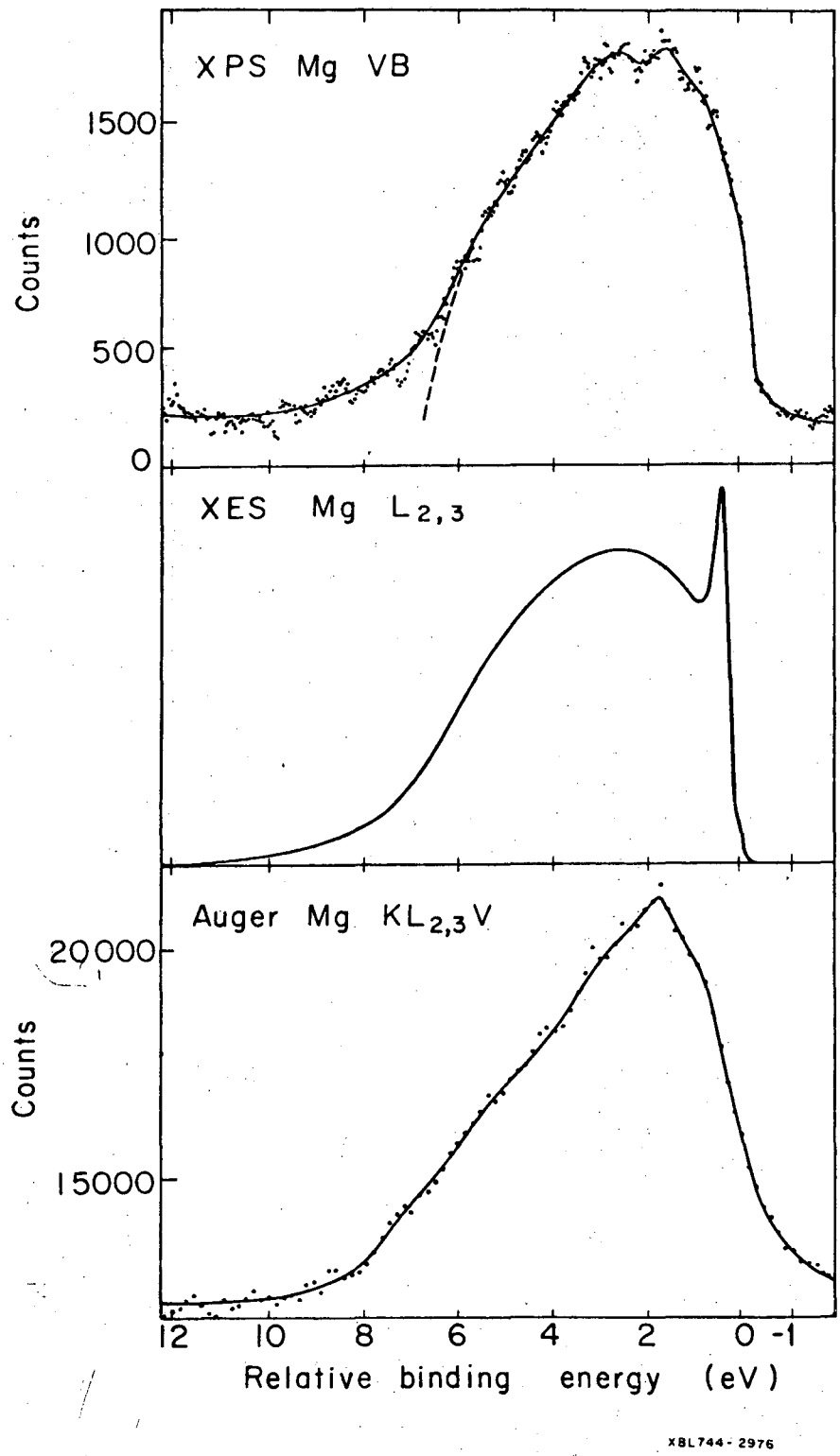
XPS Mg VB
1500
1000
500
0
Counts
XES Mg $L_{2,3}$
Auger Mg $KL_{2,3}V$
20000
15000
Counts
12
10
8
6
4
2
0
-1
Relative binding energy (eV)
XBL744-2976

Fig. 8

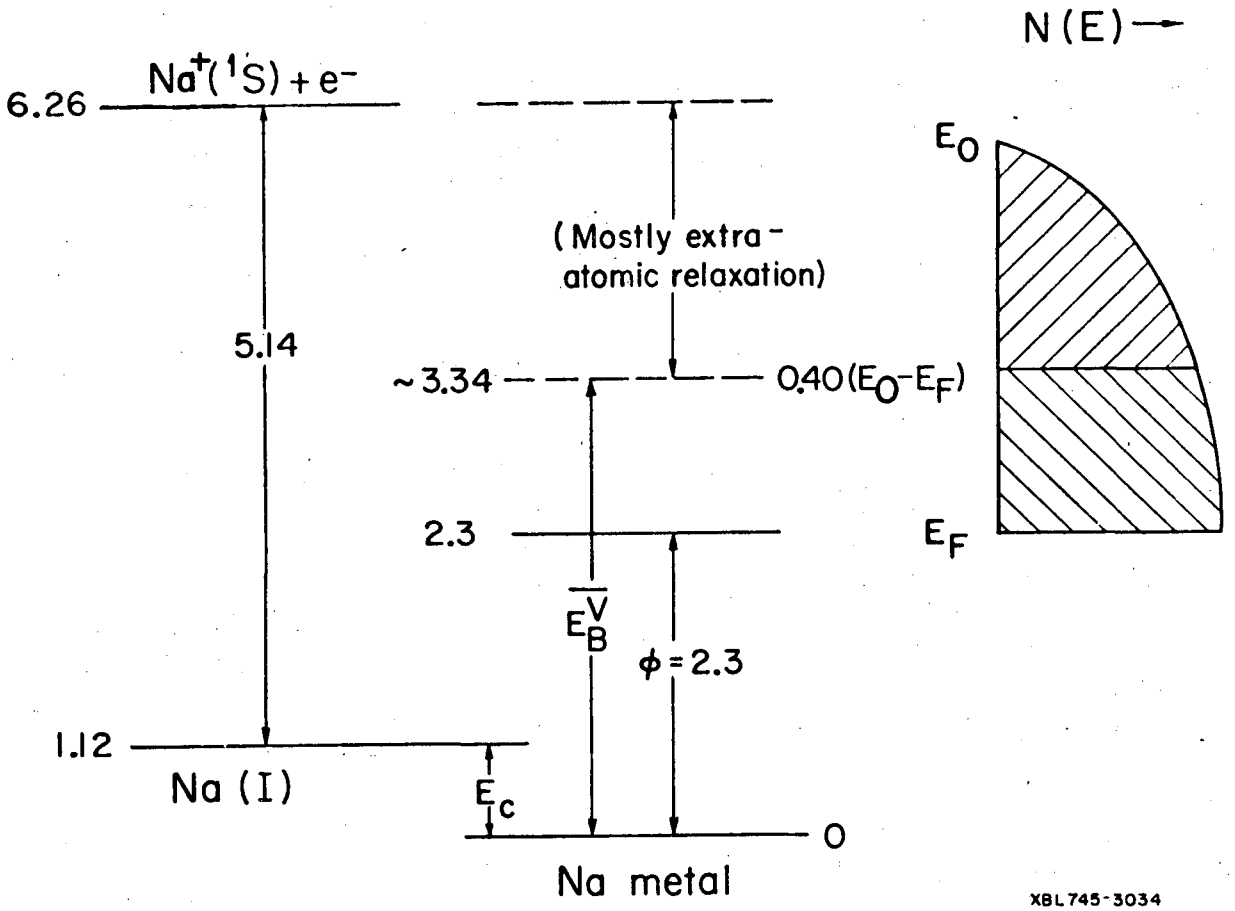
N(E)
6.26
Na+(1S) + e-
(Mostly extra-
atomic relaxation)
5.14
~3.34
0.40(E0-EF)
2.3
E0
EF
EBV
ϕ = 2.3
1.12
Na (I)
Ec
0
Na metal
XBL745-3034

Fig. 9

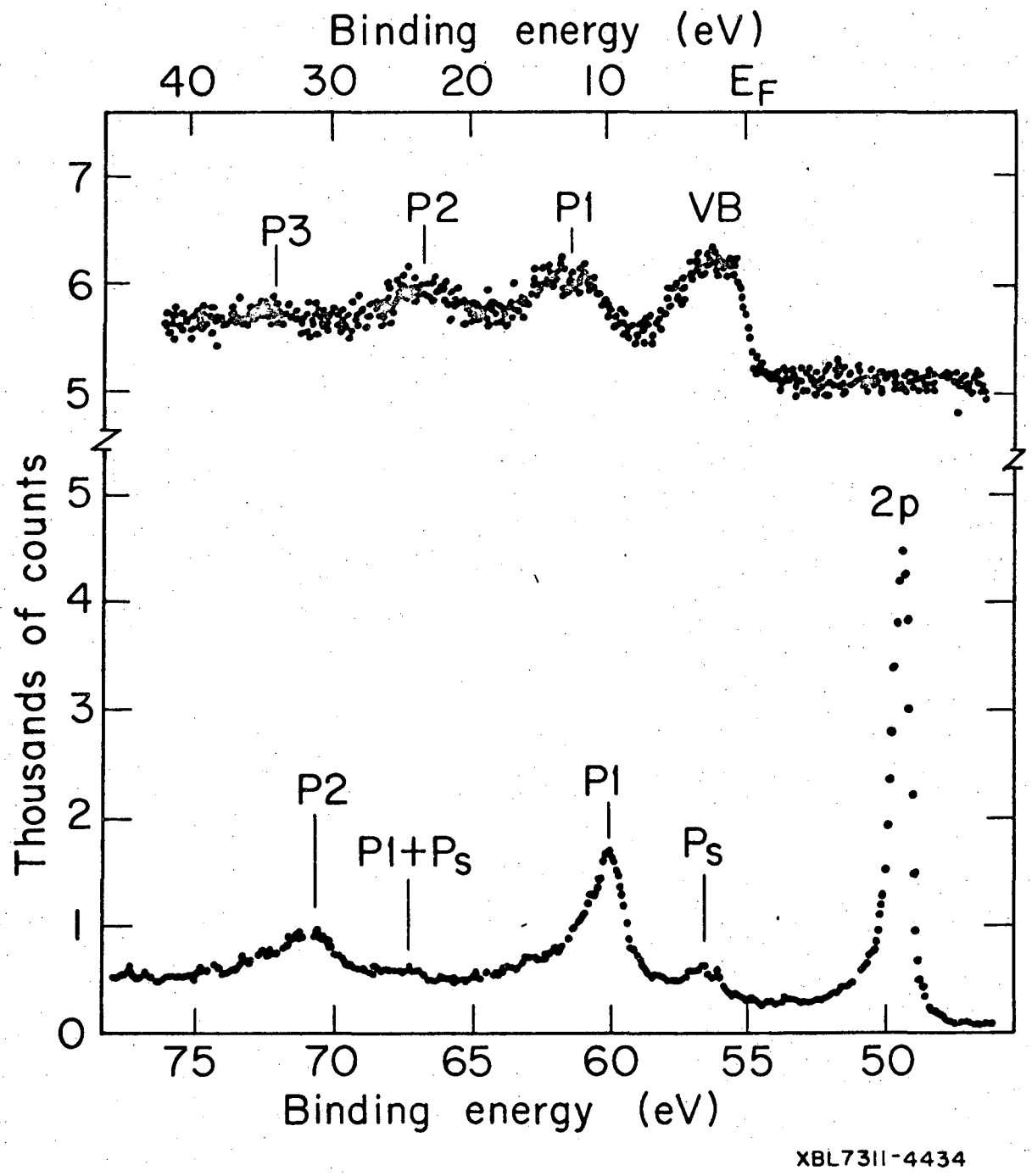
Binding energy (eV)
40
30
20
10
E_F
P3
P2
P1
VB
2p
P2
P1+Ps
P1
Ps
Thousands of counts
0
1
2
3
4
5
6
7
75
70
65
60
55
50
Binding energy (eV)
XBL7311-4434

Fig. 10

TECHNICAL INFORMATION DIVISION
LAWRENCE BERKELEY LABORATORY
UNIVERSITY OF CALIFORNIA
BERKELEY, CALIFORNIA 94720